A comparative study between CFD and FSI hemodynamic parameters in a patient-specific giant saccular cerebral aneurysm

Reza Abdollahi[1,2,3], Bahman Vahidi[1*], Pejman Shojaee[4], Mohammad Karimi[5,6]

[1] Division of Biomedical Engineering, Department of Life Science Engineering, Faculty of New Sciences and Technologies, University of Tehran, Tehran, Iran;

[2] Centre de recherche du centre hospitalier de l'Universite 'de Montr´eal (CRCHUM), Montreal, Canada;

[3] Institut de genie biomedical , Universite de Montreal, Montreal, Canada;

[4] Department of Biomedical Engineering, Division of Biomechanics, Sahand University of Technology, Tabriz, Iran;

[5] Chief of Services Stroke Neurology and Interventional Neuroradiology, Milad Hospital, Tehran,Iran;

[6] Head of Neuro-intervention, Nikan Hospital, Tehran, Iran

ABSTRACT: Nowadays, biomechanical methods are useful to identify the cause and treating of diseases. One of these diseases is the cerebral aneurysm. This disease starts by the inflation of artery wall and then by rupturing, it leads to intracranial hemorrhage. Therefore, it leads to morbidity or even it is the cause of the mortality for many patients. For this reasons, it is important to anticipate the emersion, growth and the rupture of a cerebral aneurysm. Computational fluid dynamics (CFD) and 2-way fluid-structure interaction (FSI) are common methods for interrogation the rupture of aneurysms and evaluating the effective hemodynamic parameters. In this study, they were employed to obtain appropriate information of a cerebral aneurysm. A patient-specific giant aneurysm was chosen in the internal carotid artery (ICA). Mooney-Rivlin parameters were used for the solid part and a non-Newtonian Carreu model was employed in the fluid part. Important hemodynamic parameters such as wall shear stress (WSS), time average wall shear stress (TAWSS), spatial average wall shear stress (SAWSS), oscillatory shear index (OSI), and relative residence time (RRT) were discussed. In addition, these methods were then compared and the number of cycles assessed to determine the accuracy of the solutions. Both methods illustrate a similar location for the risk of a rupture related to these hemodynamic parameters but with different quantities. The novelty of this works lies at the feasibility of using the FSI and CFD methods to show the cost function in the future clinical decision-making.

1- INTRODUCTION

Abnormal dilatations of vessels in the vascular system are called aneurysm. According to the Brain Aneurysm Foundation, cerebral aneurysms affect an estimated 6.5 million people in the United States and the annual rate of rupture is approximately 8-10 per 100,000 people. Hemodynamic parameters are considered as the main factors of the origin and progression of vascular diseases. Therefore, obtaining hemodynamic parameters led us to have a better understanding of the growth and rupture of an aneurysm, which is also helpful for anticipating the treatment's procedures [14]. In this case, particular investigations must be done for a better selection of treatment. It is necessary to propose an optimized and exact mechanical model to respond to the rate of an aneurysm arterial wall movement or to determine the exerted forces on the wall. Information must be then prepared precisely with a maximum pace. Advancements in preparing medical images and technological data have led to calculate the arterial flow in a patient-specific model by the computational analysis. It is expected that this method presents valuable information to the physicians having quantitative knowledge about the hemodynamics of a cerebral aneurysm. For this reason, it is needed to study on computational analysis, particularly by using patient-specific geometries.

Several studies have simulated the blood flow in the cerebral aneurysms by considering complicated geometries of the vessels using the computational fluid dynamic (CFD) or fluid-structure interaction (FSI) methods. However, reaching an exact framework to simulate the blood-flow in complex geometries is a challenge for the researchers. The hemodynamic properties of blood flow are playing an important role in the formation, growth and rupture of an aneurysm. Although since the results of these kind of

*Corresponding author's email: bahman.vahidi@ut.ac.ir

simulations rely on geometry, each institution reports different values of hemodynamic parameters [22]. It is still challenging to implement these parameters in clinical practice. [37] admitted that CFD could improve the anticipations and has a fundamental role in the medical treatment methods in the near future. Fluid-mechanical and morphological parameters are recognized as major factors in the rupture of human aneurysms in studies of Aranda et al.[1, 2] WSS is turned to be the biological signals via mechanoreceptors on endothelial cells, and it stimulates the cellular functions of the arterial wall. The mechanoreceptors are sensory receptors which are responding to the arterial pressure. A WSS of about 2 Pa is acceptable for preserving the structure of the aneurysm wall. However, a lower WSS led to the degeneration of endothelial cells due to the apoptotic cell cycle. An apoptotic cell cycle is defined as a shape of programmed cell death which is entailing sophisticated biochemical processes [26]. High wall Shear Stress is considered as a major parameter on the development and the growth of cerebral aneurysms [7]. Aneurysm rupture is connected to a low level of WSS and therefore it is related to a low-flow condition [30]. The aneurysm region with a low-flow condition, namely the aneurysm fundus is the dome region of an aneurysm. [36] used CFD for their simulation and showed that initially aneurysm grew in high WSS areas, then it continued to grow in areas with lower WSS. Eventually rupture occurred in areas with lower WSS. Other important parameters were also proposed in former investigations. For instance, in a research on cerebral aneurysms [6], 200 aneurysm samples were used. It is reported that the rate of viscous dissipations is based on the rupture factors of aneurysms. In the study of [38], many patients were examined with a cerebral aneurysm (more than 100 cases). It is shown that the other significant WSS parameters such as relative residence time and low shear rate are also of great importance in an aneurysm rupture.

olume changes caused by the cardiac cycle is also an important key factor to understand the hemodynamic of cerebral aneurysm. [28] compared geometric models before and after rupture and found that before rupture aneurysm volume increases intensely. Although, [19] mentioned that the data may indicate that cardiac cycle-related volume changes do not differ between unruptured aneurysms and normal intracranial arteries, suggesting that the global integrity of an unruptured aneurysmal wall is not different from that of normal intracranial arteries. [23], studied the aspect ratio statistics in an aneurysm and its relevance to the aneurysm rupture anticipation. It has been shown that the aspect ratio is the main factor in anticipating the blood flow in an aneurysm and its rupture.

In FSI method different models can be used to model the solid part. [34] compared the elastic and hyper-elastic models with 3D tetrahedral elements and they found out the differences in effective stress is 20% for elastic and 4% for the hyper-elastic model. In this study it was shown that using a linear elastic model instead of a hyperelastic material leads to an underestimation of the stress by an average of 29%. [38], employed twelve cerebrovascular aneurysms to investigate

four different viscous models comparing wall shear stress. This study was less imperative than the fluid model for average values in wall shear stress in an aneurysm case. Saqr used CFD method to analyze the differences between simplified model and non-Newtonian power-law model and a newly proposed quasi-mechanistic model. The modified Krieger model is a potential candidate for providing better clinical relevance to aneurysm CFD simulations [40]. Saeedi et al. used an FSI model to investigate 3D blood flow in an aneurysm in the circle of willis. Mooney-Rivlin model and the Carreau model have been used to consider hyperplastic property of the wall and non-Newtonian properties of the blood. They used two ideal geometry cases with only a difference between the two cases was that part of the MCA parent artery was blocked in the second case. They concluded that the risk of growth of the aneurysm is higher in cases with a partly blocked vessel [41].

Consequently, research on the blood flow dynamics inside models of cerebral aneurysms are significant to acquire quantitative criteria to specify the rupture risk of an aneurysm. By considering arterial wall properties for the computational analysis, it is needed to have exact information on the radial movement of the arterial wall. Flow waveforms are considered as inlet boundary conditions. Obtaining this information for a patient-specific model is cumbersome since the patient would not be followed by the physicians and the information could not be obtained from his/her images. The CFD method based on radiological images is one of the affordable and accessible approaches, and it is also easy to use for medical applications. Computational modeling of fluid-structure interaction is also a promising tool in modeling the complicated cardiovascular diseases as to model the blood flow inside the arteries and vessels with a vivid comprehension of the biomechanical characteristics of the arterial [4, 17]. Although it has been suggested that due to flexible structure of vessel wall, it is more realistic to use FSI method, there is not a comparison between two methods to quantitatively illustrate the differences .In this study, a patient-specific geometry is employed in a computational model to obtain information for predicting a rupture in an aneurysm and compare the FSI and CFD results. The giant cerebral aneurysm is analyzed by the CFD and FSI simulations. Results and cost function of the simulations are analyzed by quantitative analysis of the model parameters. To the best of authors knowledge, this research is one of the first studies to compare the FSI and CFD model simulations to predict the cost function and speed of calculations for a better clinical decision making.

2- MATERIALS AND METHOD
2.1. Geometry

In this study, a 56-year-old female patient with a giant saccular cerebral aneurysm was chosen for image segmentation. From the mechanical point of view, the giant aneurysm was used in the model because it has undergone more deformation than the smaller aneurysms. The spatial maximum stress ranged between 0.3 MPa in small aneurysms to 1.06 MPa in a giant aneurysm [35]. As a result of the same
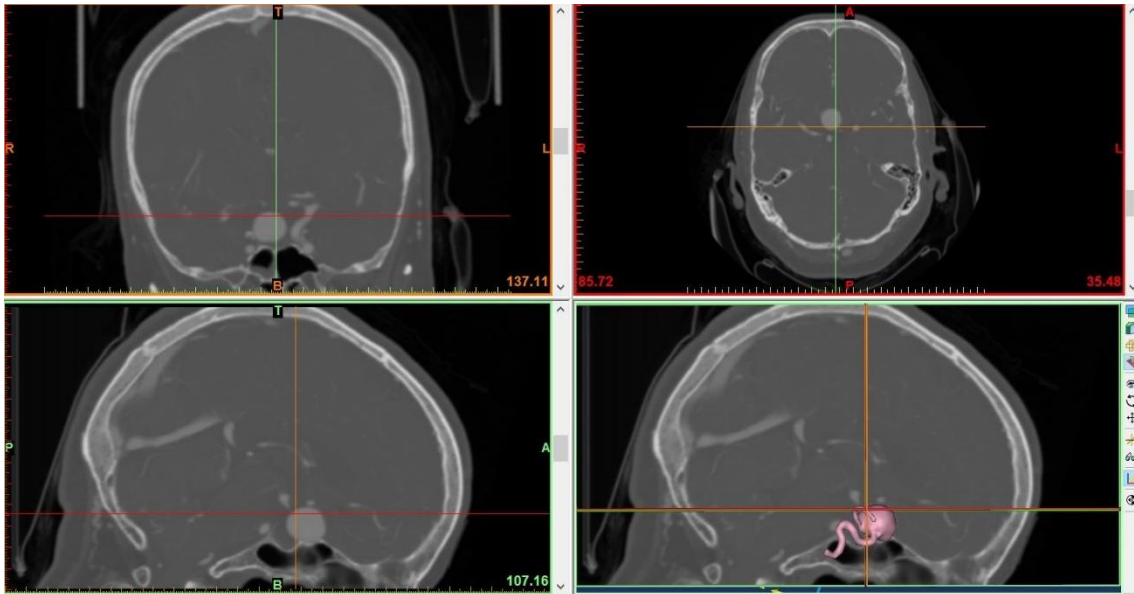
Fig. 1. The location of the patient-specific cerebral aneurysm in the CT-Angiography images in MIMICS (Materialise, Leuven, Belgium).
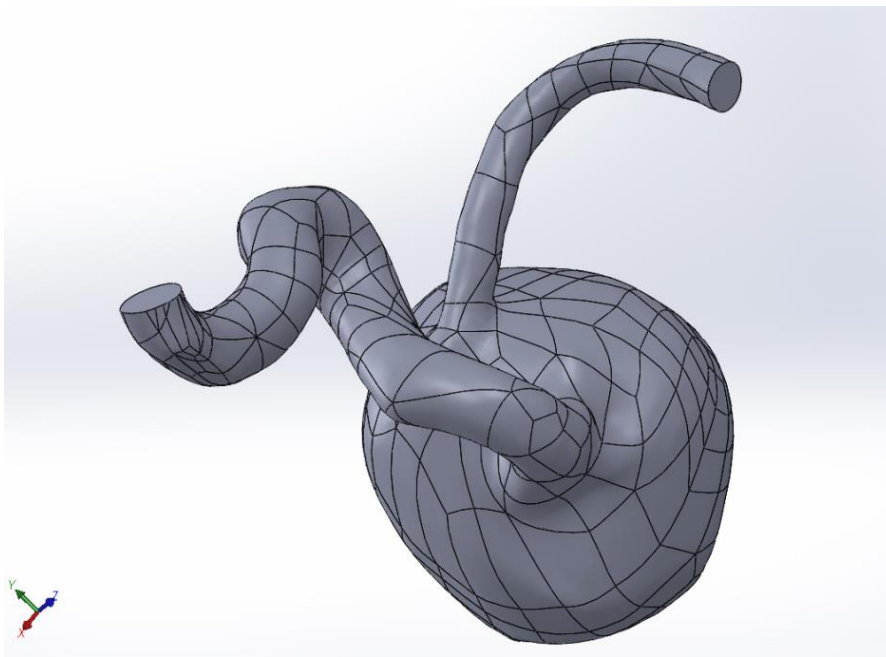
Fig. 2. The aneurysm geometry after the perpendicular cut-off at the inlet and outlet.

velocity inlet, the more deformation causes more changes in the flow pattern in the FSI simulations. The patient had a giant saccular aneurysm in the Internal Carotid Artery (ICA). These images were taken from Tooska imaging center in Iran. The resolution of images was 512×512 pixels. The depth of the aneurysm sac was 16.1 mm with the neck diameter of 10.9 mm and the aspect ratio was 1.4. The two-dimensional CT-angiography images with 233 slices with DICOM format were imported to the Mimics software 17.0 (Materialise, Leuven, Belgium) in order to extract a realistic 3D patient-specific geometric model with STL format which included the cloud points. for this purpose smooth and wrap tools had been used and the threshold was 1412 to 1610. This geometry was then imported into SolidWorks software in order to implement the boundaries (inlet and outlet flow) perpendicular to the artery. The wall thickness was considered 10% of its inlet artery diameter, so the wall thickness was 0.3 mm [32].

2.2 Fluid model

FSI method is employed in our simulations. The incompressible Navier-Stokes equations were used as the governing equation and the blood flow is assumed to be
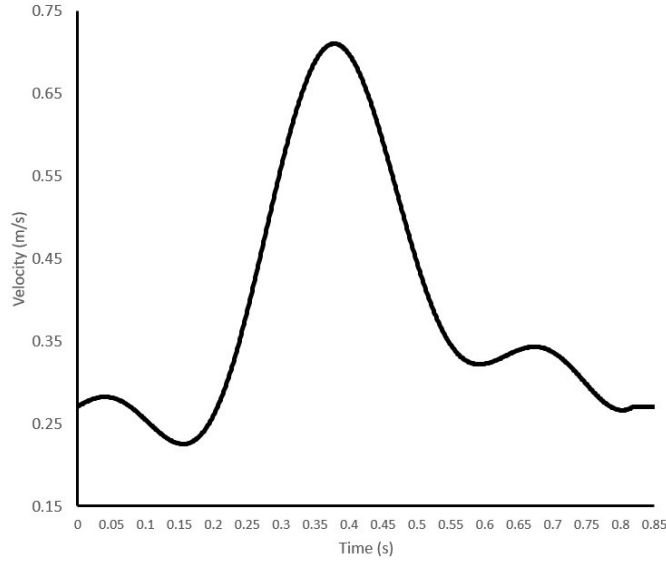
Fig. 3. Velocity inlet at each pulse of blood flow [35].

laminar [33]:

$$\nabla \cdot u = 0 \tag{1}$$

$$\frac{\partial u}{\partial t} + (u - u_g).\nabla u = \frac{\Delta p}{\rho_f} + v\Delta u \tag{2}$$

where u is the fluid velocity vector and ρ_f is the fluid density. In the Arbitrary Lagrangian-Eulerian (ALE) formulation, $u - u_g$ is the relative velocity of the fluid to the mesh. The blood is assumed as a Non-newtonian Carreau's model to show the blood properties as having shear rate at low velocities and is shown at Eq. 6 [8]:

$$\mu(\dot{\gamma}) = \mu_\infty + (\mu_0 - \mu_\infty)(1 + A\dot{\gamma}^2)^n \tag{3}$$

where μ_∞ and μ_0 are high and low shear rate viscosity asymptotic values and the parameters n and A control the transition domain size. This model prognosticates the declining of viscosity at high strain values. We use these values for these parameters as $\mu_\infty = 0.003452$ Ns/m^2 , $\mu_0 = 0.056$ Ns/m^2 , $A = 10.976$, and $n = -0.3216$. The density of blood is assumed to be constant which is equal to 1050 kg/m^3 [8].

2.3 Solid model

For the solid domain, the momentum conservation equation is considered as the governing equation which is given by Eq. 7 [33]:

$$\nabla \sigma_s = \rho_s \ddot{d}_s \tag{4}$$

where σ_s is the solid stress tensor, ρ_s is the solid density and d_s is the local acceleration of the solid. The arterial wall is assumed isotropic, incompressible, and homogeneous with a density equal to $1050 kg/m^3$ [29]. The strain energy function

for hyperelastic 5 parameters Mooney-Rivlin (ω) is shown in the following model [34]:

$$\omega(\lambda) = C_{10}(I_1 - 3) + C_{01}(I_2 - 3) + \\ C_{11}(I_1 - 3)(I_2 - 3) + C_{20}(I_1 - 3)^2 + C_{02}(I_2 - 3)^2 \tag{5}$$

where I_1 and I_2 are the first and second strain invariants of the Cauchy-Green deformation tensor C_{ij} ,respectively. $C_{ij} = 2\varepsilon_{ij} + \delta_{ij}$, where ε_{ij} is the deformation tensor δ_{ij} is the Kronecker delta, C_{10} , C_{01} , C_{11} , C_{20} , and C_{02} are material constants. In this study, the Mooney-Rivlin model is employed based on the works of [34, 9]. Five-parameters are $C_{10} = 0.3848$, $C_{01} = -0.0891$, $C_{11} = 0.5118$, $C_{20} = 0.5109$ and $C_{02} = 0.4912$ MPa [34].

2.4 Boundary conditions

The velocity profile for the inlet boundary condition is shown in Fig. 3. Since the blood flow velocity was not extracted at the same time as CT-angiogrphy and the follow up was not carried out for the patient, the boundary conditions based on the arterial location and the diameter were obtained from [35]. Traction-free boundary condition was employed at the outlet boundaries and the no-slip boundary condition was applied on the walls. On the structural part, the inlet and outlet were considered as the fixed support in order to prevent from unrealistic displacements.

2.5 Fluid-structure interactions

The Boundary conditions on the FSI interfaces forced that the dispositions of the fluid and solid domains must be correspondent and the tractions must be balanced and a no-slip condition is applied for the fluids and the conditions are as follows [33]:
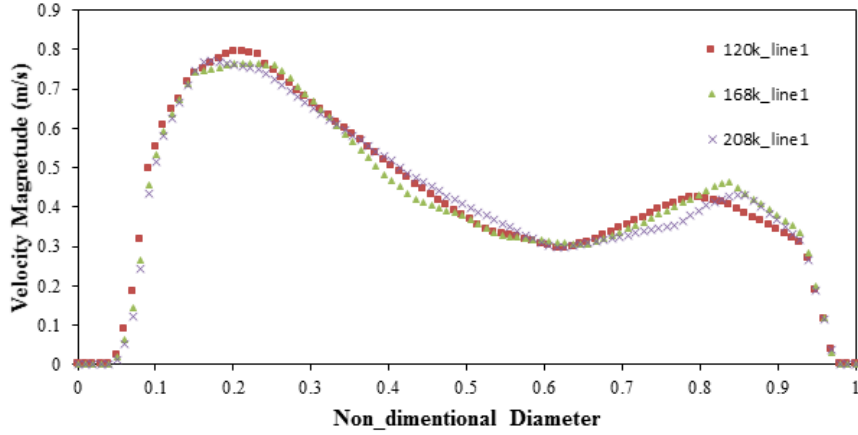
Fig. 4. Comparison of the velocity magnitude along an arbitrary line at a random time-step to check the mesh dependency

$$d_f = d_s$$
$$\sigma_f . \dot{n}_f = \sigma_s . \dot{n}_s$$
$$u_f = u_s$$

(6)

where d, σ, and $\dot{n}$ are the displacements, stress tensor, and boundary normal vectors, respectively. s and f indicate the solid and fluid, respectively. The condition for transmitting traction from fluid to solid is not required for identical matching meshes between the two domains.

2.6 Oscillatory shear index (OSI) and time-averaged wall shear stress (TAWSS)

For a pulsatile flow, TAWSS was obtained by integrating the WSS at each node over the cardiac cycle. OSI is a non-dimensional parameter which measures the directional changes of WSS during a cardiac cycle period and shows to what extent the flow tends to recirculate near the wall [31, 1]:

$$TAWSS = \frac{\int_0^T | \tau_w(t)| \, dt}{T}$$

(7)

$$OSI = 1/2 \left(1 - \frac{|\int_0^T \tau_w(t)dt|}{\int_0^T | \tau_w(t)| \, dt} \right)$$

(8)

In these equations, T_w and T are the vector of instantaneous wall shear stress and duration of the cycle, respectively. OSI values vary from 0 to 0.5. Zero is considered for steady flow and 0.5 related to the complete oscillatory flows.

2.7 Relative Residence Time (RRT)

Both high OSI and a low WSS can cause the growth and increase in rupture risk of an aneurysm; hence, it is better to present a parameter which considers both the WSS and OSI parameters. The relative residence time (RRT) was considered

for this purpose. This parameter was defined in Eq. 3. RRT could be recognized to have much more recognition than OSI since it does not have an upper limit as opposed to OSI [15]:

$$RRT = \frac{1}{(1-2OSI) \times TWASS}$$

(9)

2.8 Numerical solution

Calculations were done by five pulsatile cycles to ensure the numerical stability had been reached and the last cycle was considered as the output. The solution to the whole domain was time-dependent. The first cycle is different owing to the reason that all variables start the solution at zero. The calculations were performed on a 0.01 s time step and the time of each pulsatile cycle was considered 0.85 s. The CFD modeling is solved by the finite volume method with ANSYS Fluent 17.2 (ANSYS Inc. Canonsburg, Pa). ANSYS Mechanical solver was used for the deformation of the vessel wall and these two software packages were fully-coupled via ANSYS system coupling for the two-way FSI simulation. The formulation with large displacements and large strains in the FSI calculation were employed. Different mesh resolutions were tested to ensure the mesh independency of the geometry that included meshes with 66000, 120000, 168000, 208000 and 532000 nodes. In doing so, as shown in Fig. 4, an arbitrary line was selected to check the velocity magnitude in different mesh resolutions at a random time-step. The findings illustrated that the velocity magnitude will not be affected significantly by refining the mesh resolution more than 168000 nodes. The root mean square error between this mesh resolution and the finest mesh was 0.4735. The final choices are as follows: the computational mesh in the fluid part was constructed by the 168717 number of nodes and 395470 grids. The mesh was unstructured using tetrahedral and prism element. Five layers of prismatic cells were used in order to have an efficient numerical resolution near the wall. The
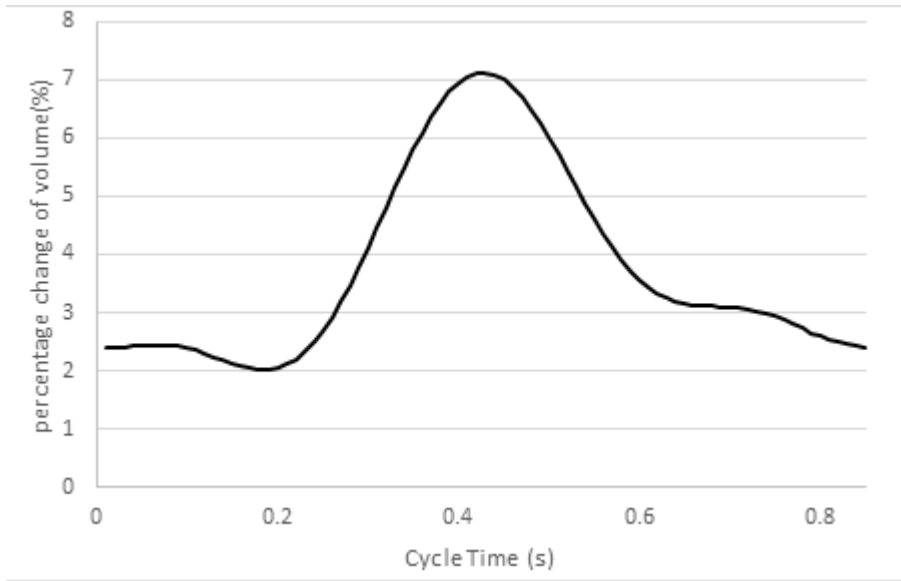
Fig. 5. percentage change of volume during a cardiac cycle
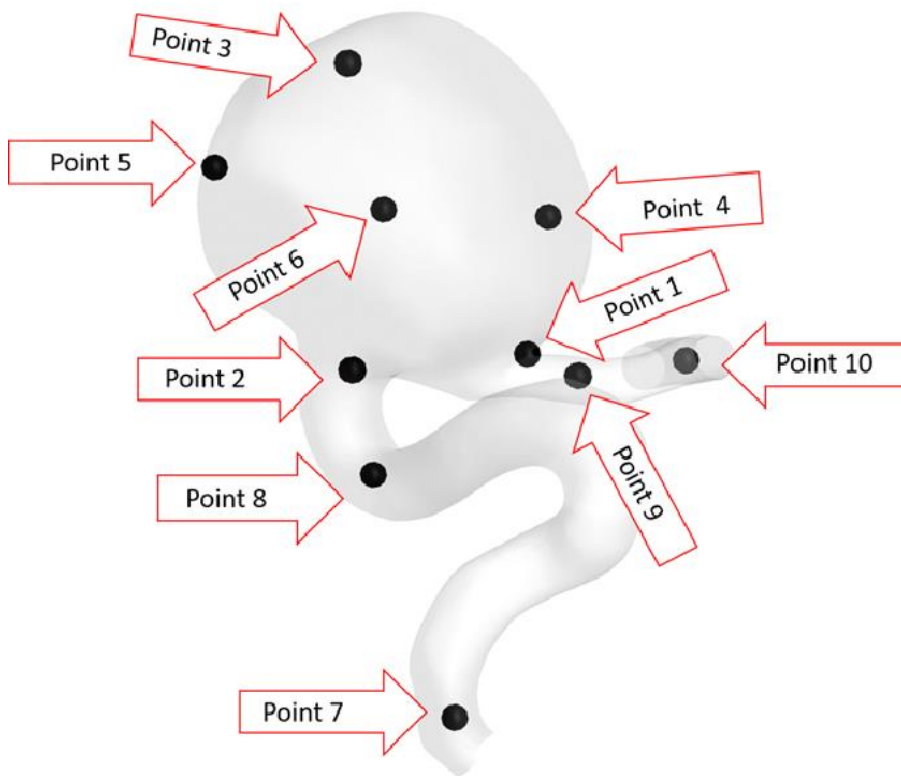
Fig. 6. Ten different points on the geometry of aneurysm

computational mesh in the solid part included 37428 nodes and 38052 elements and the type of the mesh was shell mesh as depicted in Fig. 5. The core i5 CPU Intel 4590 3.3 GHz with 8 Gb RAM memory was employed for the CFD and fully coupled FSI calculation, the calculating time for the CFD was 20 hours and for the FSI was 66 hours.

3- RESULTS
3.1 Volume

Due to nature of FSI, the arterial interior geometry changes in systole and diastole phases. The initial volume of artery interior is 4.19797 cm^3. The Fig. 6 shows the percentage change of volume during a cardiac cycle. The obtained
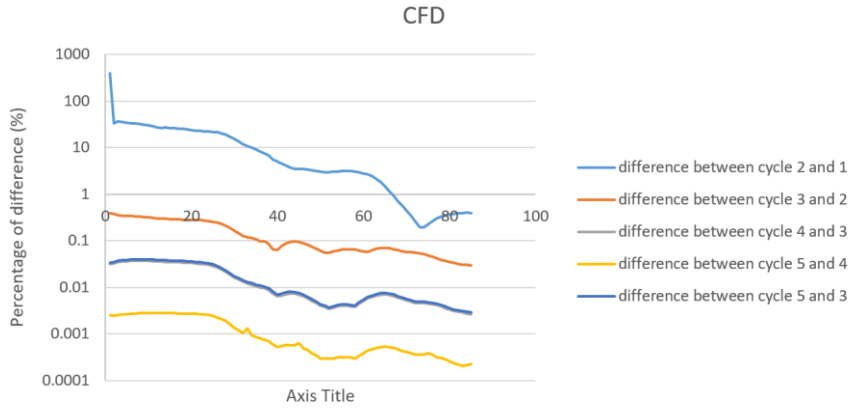
Fig. 7. The logarithmic plot of differences between the cycles in CFD solution.
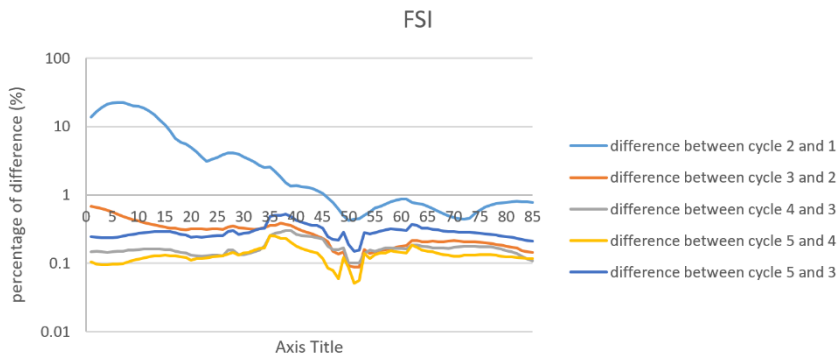
Fig. 8. The logarithmic plot of differences between the cycles in FSI simulation.
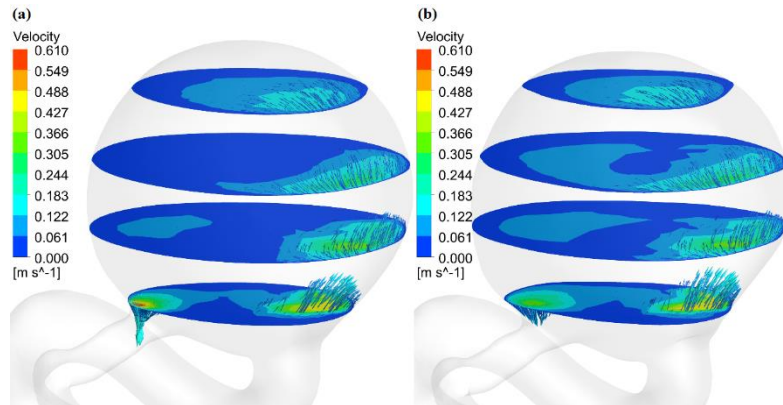
Fig. 9. contour of the blood flow velocity and the blood flow direction in 4 parallel plates at the neck of the aneurysm a) with FSI simulation b) with CFD simulation

maximum and minimum values are 4.4967 and 4.28291 cm^3 respectively and the differences between them is 4.75 %.

3.2 Differences between CFD and FSI simulations

Five different cardiac cycles were implemented in this simulation. Each cycle was 0.85 seconds and with 0.01 time step. Ten points were chosen on the geometry which you can see in Fig. 7. The data of these ten points were exported and the differences in velocity between each cycle and the cardiac cycle had been measured. As it can be seen in Fig. 8 and Fig. 9, the average of all ten points for the velocity differences in every time-step was depicted with the previous cycle. The difference between cycle 5 and 3 were exported for CFD and FSI simulations. The difference between the second and the

Table 1. The percent differences between cycles in ten points for the FSI method

	Fluid-Structure Interaction				
	cycle 2 and 1	cycle 3 and 2	cycle 4 and 3	cycle 5 and 4	cycle 5 and 3
point 1	7.3573	0.0581	0.0522	0.0554	0.1056
point 2	1.3053	0.2938	0.3315	0.2390	0.5716
point 3	1.3100	0.2938	0.3315	0.2390	0.5716
point 4	17.1800	0.1536	0.0427	0.0451	0.0765
point 5	5.0000	1.2991	0.6189	0.5325	1.1424
point 6	6.4400	0.6070	0.2063	0.1360	0.2732
point 7	0.1328	0.0070	0.0070	0.0070	0.0141
point 8	0.9962	0.0421	0.0496	0.0405	0.0883
point 9	0.8800	0.0503	0.0258	0.0300	0.0513
point 10	6.0828	0.0068	0.0063	0.0039	0.0086
all points	4.6674	0.2812	0.1672	0.1328	0.2903

Table 2. The percent differences between cycles in ten points for the CFD method

	Computational Fluid Dynamic				
	cycle 2 and 1	cycle 3 and 2	cycle 4 and 3	cycle 5 and 4	cycle 5 and 3
point 1	0.9020	0.0080	0.0012	0.0001	0.0013
point 2	1.2995	0.0056	0.0003	2.4700	0.0003
point 3	40.6852	0.4101	0.0214	0.0014	0.0200
point 4	38.5711	0.4327	0.0145	0.0009	0.0154
point 5	39.9337	0.2304	0.0452	0.0036	0.0488
point 6	32.1026	0.3559	0.0656	0.0054	0.0711
point 7	0.2486	2.2100	2.1800	1.0600	2.4000
point 8	0.4768	2.5900	1.8500	1.3700	2.4800
point 9	1.4260	0.0186	0.0023	0.0002	0.0006
point 10	0.8823	0.0064	0.0005	0.0001	0.0006
all points	15.6528	0.1468	0.0151	0.0012	0.0163

first cycle was more than 1% in both simulations.

The same amount was also observed for the percent difference between third and the fifth cycle and the third and fourth cycle. Table. 1 shows the difference in WSS between different cycles. It is obvious that the highest difference between the second and first cycle was related to the inside the Aneurysm sac. This shows that the analysis of inside of the aneurysm sac was more complex which depicted the importance of the patient-specific geometry. The CFD simulation got 0.1 times more accurate in each cycle.

Fig. 8, shows that the difference in the second and first cycle was more than 1%. However, according to the Fluent's solver and its system coupling with mechanical transient; the first cycle's data approaches earlier than the fifth cycle's data (after the 45th step which for the CFD was after the 66th step) shows the primacy of the FSI to the CFD solution.

After the cycle 3,4, and 5 the differences were negligible, these amounts were less than 1%. The difference was also less than 1% for the cycle 5 from cycle 3. Table. 1, shows this issue is exclusively for the difference of cycle 3 to cycle 2. The point 5 had been chosen close to aneurysm sac's wall and the most differences were related to this point since the geometry changes and aneurysm wall displacement. It

could be concluded that the difference in the CFD solution between the three and five cycles were less than 0.05% which means a little difference. The percent difference was also less than 0.5% for the FSI solution which was negligible, (Fig. 9). Therefore, it would be cost effective for the two solutions if we consider the three cycles and for the higher accuracy use a higher quality mesh.

3.3 Velocity

Fig. 10 shows the velocity field at the peak of systole in which 4 parallel planes (planes parallel to the neck of an aneurysm) were considered. In the CFD and FSI simulations, first, the flow entered the aneurysm sac, and then distributed. In the end, the amount of velocity was reduced at the exit (outlet). The flow entered to the aneurysm occupied a small part of the whole aneurysm's volume; meanwhile, in the most of the aneurysm sac's volume, the flow was at the downstream vessels. Jet flows appeared at the entrance of aneurysm sac by the high-velocity profiles. This jet flow caused a high WSS at the wall close to the parent artery entrance. In the FSI simulation, the flow from the aneurysm sac caused high velocity at the entrance of the parent artery which produced concentrated flows at the beginning of the arterial outlet.

3.4 Wall Shear Stress
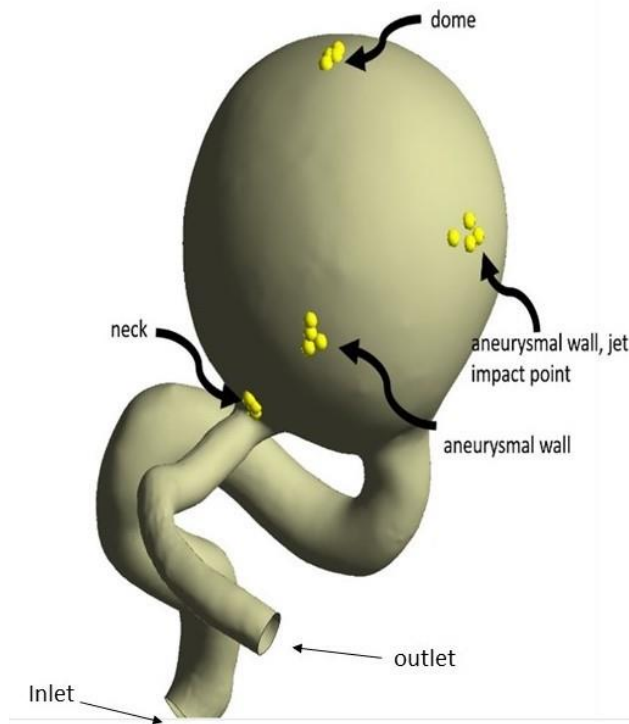
Fig. 10. The position of the dome, neck, aneurysmal wall, jet impact point
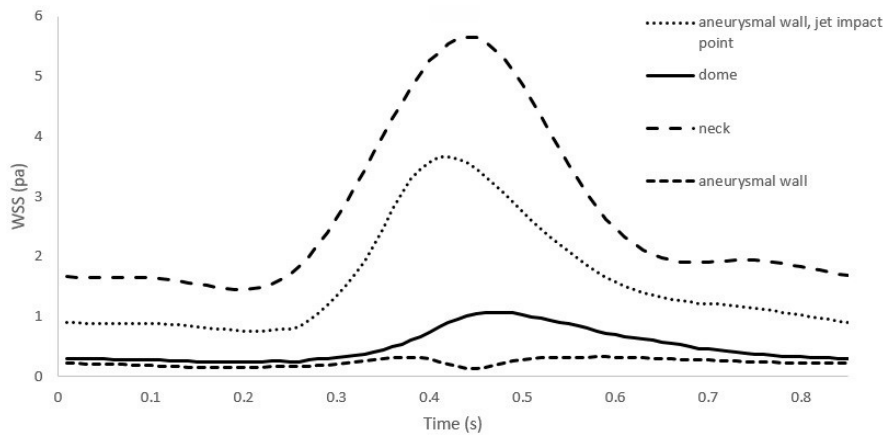
Fig. 11. The averaged WSS at the dome, neck, aneurysmal wall, jet impact point

Four regions are illustrated to determine differences of the wall shear stress (WSS) in the FSI method. For each region, the average of four close nodes was determined (Fig. 11). The maximum amount of WSS occurred at the 4.4 s, 4.7 s, 5.9 s, and 4.2 s for the neck, the dome, aneurysmal wall, and the aneurysmal wall, jet impact point, respectively. It is shown in Fig. 12 that the high shear stress at the neck of the aneurysm was due to the high-velocity flow at this point. The flow on the aneurysmal wall was completely independent of the inlet flow. The downstream flow had effects subsequently inside the aneurysm; the highest WSS was for the jet impact point and the aneurysm sac.

Fig. 13 shows the spatial average of wall shear stress (SAWSS) for two FSI and CFD methods at the 3rd and 5th cycles. There are two main differences between the SAWSS in FSI and CFD methods. First, the maximum SAWSS has been shifted to 0.43 s in the FSI simulation, whereas in the CFD method it occurs at 0.38 s. In addition, the maximum inlet velocity happened at 0.38 s. The time delay in the FSI simulation could be explained by the wall movement which has affected the velocity and WSS. Second, the maximum SAWSS was 20 percent lower in the FSI simulation. The differences between the 5th and 3rd cycles was very low and in the CFD simulation the difference was plummet to the 0.0002 percent in which the 0.4 percent was reported for the FSI.

For the time average of WSS (TAWSS), there were no significant differences between the FSI and CFD models. This is because of the type of distribution of shear stress on the wall
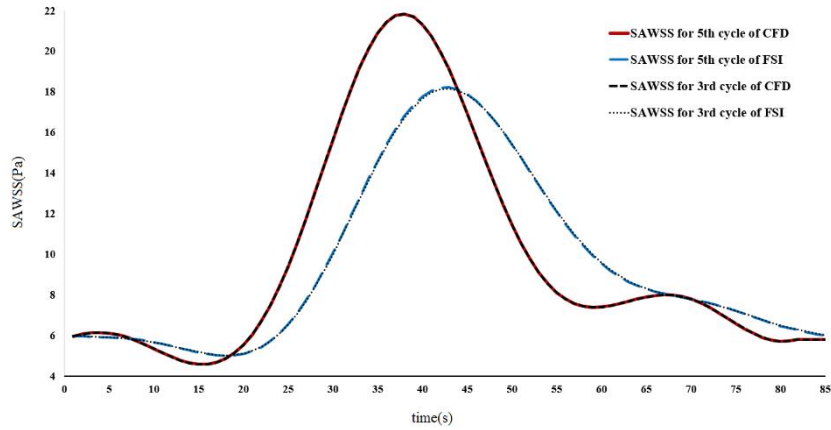
Fig. 12. Comparison between the spatial average wall shear stress for CFD and FSI simulations
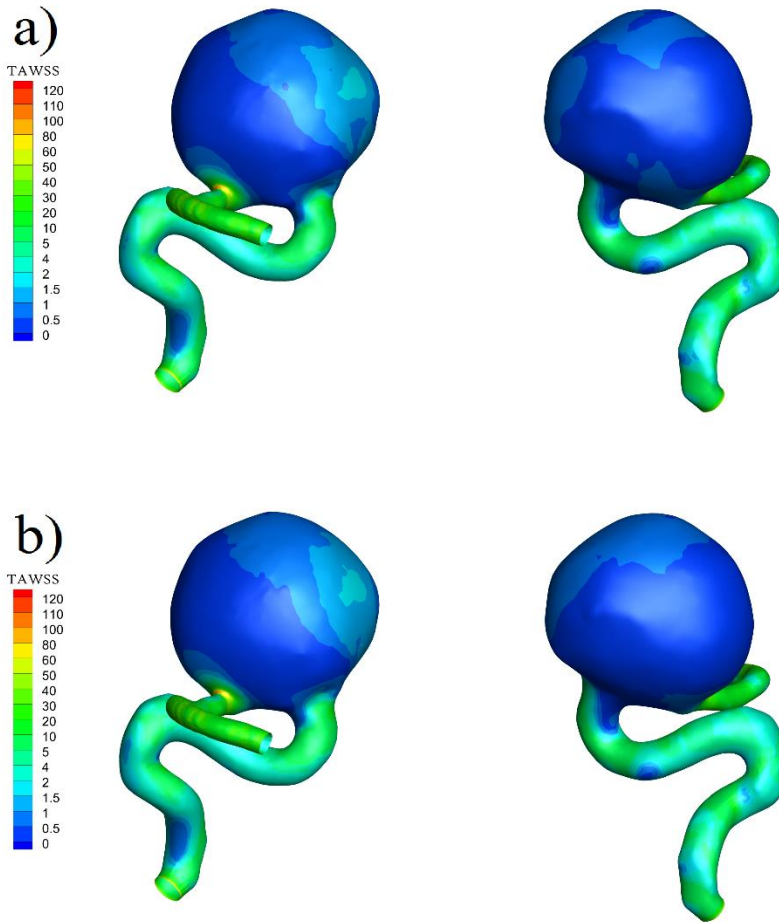
Fig. 13. Time-averaged wall shear stress a) for the CFD simulation and b) for the FSI simulation. For better illustration, counters are plotted from two views.

which was similar in both FSI and CFD methods. Because of the specific anatomy of the patient, a lower diameter at the arterial outlet existed rather than at an aneurysm sac, owing to the maximum value of this parameter occurred at the outlet boundary of the aneurysm sac, as it is shown in Fig. 14. This

also led to a higher velocity of the flow at the outlet.

On the sac wall, the time average wall shear stress was insignificant due to the weak flow toward the arterial outlet of the aneurysm sac.

3.5 OSI

As it is shown in Fig. 15, OSI parameter was depicted
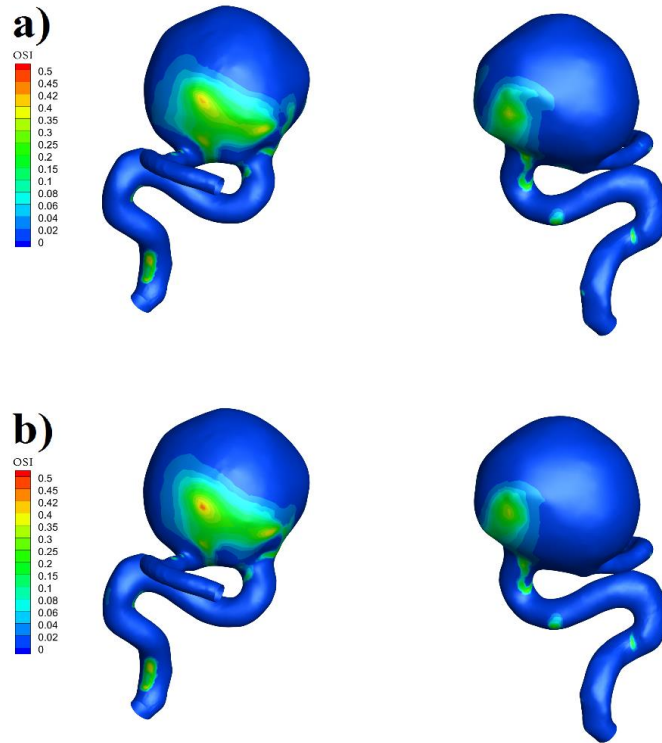
Fig. 14. Oscillatory shear factor (OSI); a) for the CFD simulation, and b) for the FSI simulation. For better illustration, counters are plotted from two views.
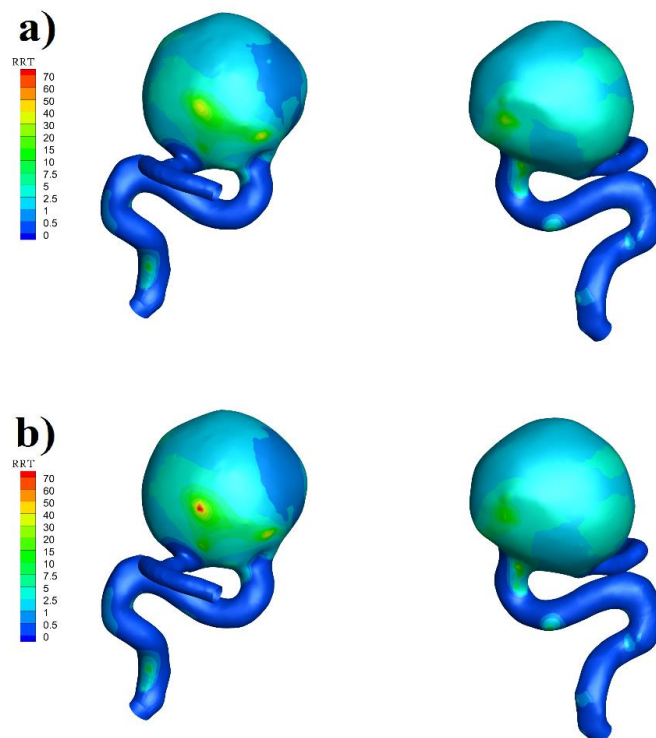
Fig. 15. Relative residence time; a) for the CFD simulation and b) for the FSI simulation. For better illustration, counters are plotted from two views.

for the CFD and FSI methods on two different angles. The amount range of this parameter is from 0 to 0.5. In the FSI solution, the maximum value of this parameter was more

than the value in the CFD solution. At the intact artery part, because of the vicinity to the inlet flow, the effect of this parameter was negligible, whereas this parameter could be

affected at the neck inlet of an aneurysm and on the wall of the aneurysm sac; therefore the flow hit the wall after entering to the aneurysm sac. This region tends to be ruptured based on the medical observations [29].

3.6 RRT

As it is shown in Fig. 16, it is observed that the maximum amount of RRT parameter is twice for the FSI solution as compared to the magnitude of this parameter in the CFD solution. The regions of the wall where the flow changes significantly, cause a high amount of RRT and represent a high OSI and low shear stress. These regions are the most plausible points for the endothelial cell stimulation. As is shown in Fig. 16, these points occurred at the entrance of the flow at the aneurysm sac. The difference between the values in these two models implies that the CFD and FSI solutions have the same regions in maximum relative RRT but with different values.

In general the blood velocity at the entrance and the maximum value of OSI and RRT were higher in the FSI simulation. Our results showed that maximum SAWSS is 20% lower in FSI method and occurs later in the cardiac cycle. TAWSS was similar in both methods. Also it is worth mentioning that maximum RRT was observed at the sama area.

4- DISCUSSION

A specific case was selected from patients that had a cerebral aneurysm. An aged female with a giant saccular cerebral aneurysm at the internal carotid artery was chosen. The CT-angiography images showed that the aneurysm sac enlargement can put pressure on the III and VI cranial nerves due to the location of the aneurysm. Computational fluid dynamics (CFD) could be a strong tool for analyzing and interpreting the cerebral vessel diseases such as ruptured and unruptured cerebral aneurysms. With the aid of this tool, valuable information about effective parameters in this field is achievable without any invasive risk [29]. However, no biological data was employed and only morphological data had been used without the actual blood pressure, blood viscosity, and the drainage change in the biological parameters which shows the limitation of CFD studies [22]. Moreover, results of fully two way fluid-structure interaction (FSI) which used CFD and computational structural dynamics (CSD), are more realistic than the solely CFD results owing to the consideration of the displacements of the wall that has effects on the blood flow.

Recent studies have depicted that the involvement and progress of WSS in the formation of saccular cerebral aneurysms is significant [18]. When the velocity of flow is increased, this causes an increase in WSS, motivates the release of endothelium-derived nitrous oxide which is renowned as a strong vasodilator and a powerful factor in arterial wall degeneration [12]. The cellular regeneration is influenced by the low WSS. Both high and low WSS cause the degradation of the extracellular matrix (ECM) and cell death [21]. The high oscillatory shear stress index influences the endothelial function which is connected to the increase of Endothelia-1

(ET-1) and a decrease of NOx productions and at the end, it has the ability to cause the cellular toxicity and smooth muscle cell proliferation and atherogenesis [39]. This dysfunction is measured by OSI which is shown in Fig.15. [13] found that the ruptured area of the aneurysms spatially related to the area through the jet flow enters the aneurysm and hit its wall. This area also corresponded to the adjacent fluid which is induced by WSS in the aneurysms. Some researchers reported that low wall shear stress plays a significant role as a risk factor for aneurysm rupture [20, 11, 25]. When the complex flow with multiple vortices is created in the aneurysm sac, the flow adjacent to the walls tends to be recirculating, slow and oscillatory. So, in these regions, WSS has a low amount and OSI has a high value and fluid particles tend to spend a long time near the wall [20]. It was reported that the formation of an aneurysm is highly related to the OSI [29, 5]. High OSI cause inflammatory-cell-mediated destructive remodeling [21].

[24] have reported that non-Newtonian effects of the blood is significant and must be considered in cerebral aneurysms owing to the low velocity flow in the aneurysm dome and low-scale cerebral vessels. In addition, in the FSI method, we deal with the velocity wall movement which is slower than the fluid flow at the middle of the artery. So, in this study, the blood is assumed as a Non-newtonian carreauâ€™s model. Previous studies have shown that the assumption of the rigid wall for modeling the elastic properties of the vessels wall overestimates WSS [16]. However, in this study, a hyperelastic property of the vessels wall is employed which undermine the magnified effect of WSS on the wall owing to the higher deformation.

In this research we aim to compare the cost function of CFD and FSI methods in 3rd and 5th cycles to show the properties for the specific uses. FSI method is a precise tool for studying the changes in the flow pattern near the wall by considering the wall movement, meanwhile, CFD tool is an appropriate tool to see the flow pattern a bit far from the wall. In fact in CFD analysis the flow is distributed to the mostly middle of aneurysmal sac, while in FSI analysis the blood flow is close to the wall, which transfers energy from fluid to the wall and deforms it, so it has more effect on the WSS. For anticipating the fluid dynamics inside the aneurysm, the assumption of FSI illustrates a significant effect in WSS on the aneurysm; the difference between CFD and FSI, in prediction of WSS is 18% and the flow pattern in FSI and CFD analysis has minor differences. In fig. 11 the jet impact point has been shown. The jet impact point has more TAWSS compared to other regions on aneurysmal wall (Fig. 14). But as shown in fig. 15 and Fig. 16 the OSI and RRT are lower than other regions of the aneurysmal wall. It is abounds eventing the jet impact point has more WSS but the risk of rupture is less than other regions and the reason is that the direction of WSS in this region is not changing much and only the amount is changing due to heart beat.

OSI has been widely used to identify the regions experiencing flow separation, which leads to the creation of a recirculation zone[1-18,28] The areas of high OSI and lower

TAWSS values are consistent with the recirculation areas corresponding to the aneurysm growth zone. In the results for the OSI in the FSI solution, the maximum value of this parameter is more in the value of the CFD solution. In Fig. 16, it is clear that the high amount of RRT parameter is related to the regions with the low movement of blood particles which are almost quiescent in those areas [35, 24]. When the aneurysm rupture happens, the effective stress (flow-induced stress) exceeds the strength of the aneurysmal wall [27]. It is found that the strength of the wall is related to the collagen fibers, strength and their directions in the aneurysm wall [34].

To validate the model, clinical studies are the most needed items. However, it is decisive to bring biomechanically based aneurysm risk assessment towards the clinical practice. While validation is a complicated term because of the lack of standard method and rare clinical event rate to estimate the risk. Nonetheless, our model shows a good agreement with the studies [10, 3] on the wall shear stress and OSI. Also the calculated cardiac cycle-related volume is 4.75% which is in good agreement with the study done by [19]. They used Four-dimensional CT angiography for 18 patients and found out that The cardiac cycle-related volume changes of the intracranial aneurysms and intracranial normal arteries were $5.40\% \pm 4.17\%$ and $4.20 \pm 2.04\%$, respectively. As shown in fig. 13 changes in the volume alter the flow distribution and can affect the WSS. Therefore studying the volume change is an important task.

Since there was no clinical data available, this study was limited by the absence of comparison of velocity field and pressure distribution obtained from numerical simulation and physiological data. Also the lack of follow up made it difficult to estimate the volume change during cardiac cycle and to determine the exact area on the aneurysm sac that rupture occurs. In addition, using images with higher resolution and more realistic model for the solid part can improve the accuracy of the numerical findings. Another potential limitation is that only one patient data set was used. Also it should be mentioned that the traction-free boundary condition was specified at the outlets and since patient-specific measured waveform was not available, we used a conventional velocity waveform (applied at the inlet of the parent artery) from a patient similar to our studied case with a CA located in the internal carotid artery.

5- CONCLUSION

In this research, CFD and FSI simulations were investigated for a patient-specific giant saccular cerebral aneurysm located at the internal carotid artery. The model was obtained from CT-Angiography image data. However, it is not known that which factor can predict the rupture more accurately. In this study, we try to compare some of the these factors in both simulation. There are important points for considerations in this study such as the wall deformation since a giant aneurysm put pressure on the III and IV cranial nerves which could be affected and led to nervous system damages. Five cycles had been carried out and the differences between the circles in FSI and CFD were depicted. We determined that 3 cycles for the

CFD simulation is quiet enough since the differences between the 5 and 3 cycles is less than 0.1%. In addition, 30% of cost function would be reduced for the FSI simulation with the 3 cycle. This is because of the low percentage difference (less than 1%) between 3 and 5 cycle. Several parameters such as velocity, WSS, TAWSS, OSI, and RRT were also studied and the differences between the CFD and FSI methods were shown. Two main points can be derived from this study. First, CFD simulation which is cost-effective showed the different quantity of these parameters. WSS and OSI were higher than the values obtained from the FSI simulation. Second, the difference between the values in these two models implies that the CFD and FSI solutions have the same regions in the maximum of RRT but different values for this parameter.

CONFLICT OF INTEREST

The authors declare that they have no conflicts of interest.

REFERENCES

[1] A. Aranda, A.J.M.L. Valencia, A.A.I.J. Vol, Study on cerebral aneurysms: Rupture risk prediction using geometrical parameters and wall shear stress with cfd and machine learning tools, 5 (2018).

[2] A. Aranda, A.J.J.o.M.i.M. Valencia, Biology, Computational study on the rupture risk in real cerebral aneurysms with geometrical and fluid-mechanical parameters using FSI simulations and machine learning algorithms, 19(03) (2019) 1950014.

[3] X. Bai-Nan, W. Fu-Yu, L. Lei, Z. Xiao-Jun, J.J.N.r. Hai-Yue, Hemodynamics model of fluid–solid interaction in internal carotid artery aneurysms, 34(1) (2011) 39-47.

[4] H.-J. Bungartz, M. Schäfer, Fluid-structure interaction: modelling, simulation, optimisation, Springer Science & Business Media, 2006.

[5]] A. Can, R.J.N. Du, Association of hemodynamic factors with intracranial aneurysm formation and rupture: systematic review and meta-analysis, 78(4) (2016) 510-520.

[6] J.R. Cebral, F. Mut, J. Weir, C.J.A.J.o.N. Putman, Quantitative characterization of the hemodynamic environment in ruptured and unruptured brain aneurysms, 32(1) (2011) 145-151.

[7] I. Chatziprodromou, A. Tricoli, D. Poulikakos, Y.J.J.o.b. Ventikos, Haemodynamics and wall remodelling of a growing cerebral aneurysm: a computational model, 40(2) (2007) 412-426.

[8] Y.I. Cho, K.R.J.B. Kensey, Effects of the non-Newtonian viscosity of blood on flows in a diseased arterial vessel. Part 1: Steady flows, 28(3-4) (1991) 241-262.

[9] V. Costalat, M. Sanchez, D. Ambard, L. Thines, N. Lonjon, F. Nicoud, H. Brunel, J.P. Lejeune, H. Dufour, P.J.J.o.b. Bouillot, Biomechanical wall properties of human intracranial aneurysms resected following surgical clipping (IRRAs Project), 44(15) (2011) 2685-2691.

[10] K.D. Dennis, D.F. Kallmes, D.J.J.o.b. Dragomir-

Daescu, Cerebral aneurysm blood flow simulations are sensitive to basic solver settings, 57 (2017) 46-53.

[11] K. Fukazawa, F. Ishida, Y. Umeda, Y. Miura, S. Shimosaka, S. Matsushima, W. Taki, H.J.W.n. Suzuki, Using computational fluid dynamics analysis to characterize local hemodynamic features of middle cerebral artery aneurysm rupture points, 83(1) (2015) 80-86.

[12] R.J. Guzman, K. Abe, C.K.J.S. Zarins, Flow-induced arterial enlargement is inhibited by suppression of nitric oxide synthase activity in vivo, 122(2) (1997) 273-280.

[13] T. Hassan, E.V. Timofeev, T. Saito, H. Shimizu, M. Ezura, T. Tominaga, A. Takahashi, K.J.A.j.o.n. Takayama, Computational replicas: anatomic reconstructions of cerebral vessels as volume numerical grids at three-dimensional angiography, 25(8) (2004) 1356-1365.

[14] B. Hillen, T. Gaasbeek, H.W.J.J.o.b. Hoogstraten, A mathematical model of the flow in the posterior communicating arteries, 15(6) (1982) 441-448.

[15] H.A. Himburg, D.M. Grzybowski, A.L. Hazel, J.A. LaMack, X.-M. Li, M.H.J.A.J.o.P.-H. Friedman, C. Physiology, Spatial comparison between wall shear stress measures and porcine arterial endothelial permeability, 286(5) (2004) H1916-H1922.

[16] J.G. Isaksen, Y. Bazilevs, T. Kvamsdal, Y. Zhang, J.H. Kaspersen, K. Waterloo, B. Romner, T.J.S. Ingebrigtsen, Determination of wall tension in cerebral artery aneurysms by numerical simulation, 39(12) (2008) 3172-3178.

[17] J. Janela, A. Moura, A.J.J.o.C. Sequeira, a. Mathematics, A 3D non-Newtonian fluid–structure interaction model for blood flow in arteries, 234(9) (2010) 2783-2791.

[18] S. Kondo, N. Hashimoto, H. Kikuchi, F. Hazama, I. Nagata, H.J.S. Kataoka, Cerebral aneurysms arising at nonbranching sites: an experimental study, 28(2) (1997) 398-404.

[19] J. Kuroda, M. Kinoshita, H. Tanaka, T. Nishida, H. Nakamura, Y. Watanabe, N. Tomiyama, T. Fujinaka, T.J.S. Yoshimine, Cardiac cycle-related volume change in unruptured cerebral aneurysms: a detailed volume quantification study using 4-dimensional CT angiography, 43(1) (2012) 61-66.

[20] G. Lu, L. Huang, X. Zhang, S. Wang, Y. Hong, Z. Hu, D.J.A.J.o.N. Geng, Influence of hemodynamic factors on rupture of intracranial aneurysms: patient-specific 3D mirror aneurysms model computational fluid dynamics simulation, 32(7) (2011) 1255-1261.

[21] H. Meng, V. Tutino, J. Xiang, A.J.A.J.o.N. Siddiqui, High WSS or low WSS? Complex interactions of hemodynamics with intracranial aneurysm initiation, growth, and rupture: toward a unifying hypothesis, 35(7) (2014) 1254-1262.

[22] Y. Murayama, S. Fujimura, T. Suzuki, H.J.N.f. Takao, Computational fluid dynamics as a risk assessment tool for aneurysm rupture, 47(1) (2019) E12.

[23] A. Nader-Sepahi, M. Casimiro, J. Sen, N.D.J.N. Kitchen, Is aspect ratio a reliable predictor of intracranial aneurysm rupture?, 54(6) (2004) 1343-1348.

[24] M. Ohta, S.G. Wetzel, P. Dantan, C. Bachelet, K.O. Lovblad, H. Yilmaz, P. Flaud, D.A.J.C. Rüfenacht, i. radiology, Rheological changes after stenting of a cerebral aneurysm: a finite element modeling approach, 28(6) (2005) 768-772.

[25] S. Omodaka, S.-i. Sugiyama, T. Inoue, K. Funamoto, M. Fujimura, H. Shimizu, T. Hayase, A. Takahashi, T.J.C.D. Tominaga, Local hemodynamics at the rupture point of cerebral aneurysms determined by computational fluid dynamics analysis, 34(2) (2012) 121-129.

[26] L. Pentimalli, A. Modesti, A. Vignati, E. Marchese, A. Albanese, F. Di Rocco, A. Coletti, P. Di Nardo, C. Fantini, B.J.J.o.n. Tirpakova, Role of apoptosis in intracranial aneurysm rupture, 101(6) (2004) 1018-1025.

[27] A. Robertson, P. Watton, Computational fluid dynamics in aneurysm research: critical reflections, future directions, in, Am Soc Neuroradiology, 2012.

[28] J. Schneiders, H. Marquering, R. Van den Berg, E. VanBavel, B. Velthuis, G. Rinkel, C.J.A.J.o.N. Majoie, Rupture-associated changes of cerebral aneurysm geometry: high-resolution 3D imaging before and after rupture, 35(7) (2014) 1358-1362.

[29] A. Shamloo, M.A. Nejad, M.J.J.o.t.m.b.o.b.m. Saeedi, Fluid–structure interaction simulation of a cerebral aneurysm: Effects of endovascular coiling treatment and aneurysm wall thickening, 74 (2017) 72-83.

[30] M. Shojima, M. Oshima, K. Takagi, R. Torii, M. Hayakawa, K. Katada, A. Morita, T.J.S. Kirino, Magnitude and role of wall shear stress on cerebral aneurysm: computational fluid dynamic study of 20 middle cerebral artery aneurysms, 35(11) (2004) 2500-2505.

[31] A. Swillens, M. De Witte, H. Nordgaard, L. Løvstakken, D. Van Loo, B. Trachet, J. Vierendeels, P.J.M. Segers, b. engineering, computing, Effect of the degree of LAD stenosis on "competitive flow" and flow field characteristics in LIMA-to-LAD bypass surgery, 50(8) (2012) 839-849.

[32] R. Torii, M. Oshima, T. Kobayashi, K. Takagi, T.E.J.C.M. Tezduyar, Fluid–structure interaction modeling of aneurysmal conditions with high and normal blood pressures, 38(4) (2006) 482-490.

[33] A. Valencia, F.J.I.C.i.H. Baeza, M. Transfer, Numerical simulation of fluid–structure interaction in stenotic arteries considering two layer nonlinear anisotropic structural model, 36(2) (2009) 137-142.

[34] A. Valencia, P. Burdiles, M. Ignat, J. Mura, E. Bravo, R. Rivera, J.J.C. Sordo, m.m.i. medicine, Fluid structural analysis of human cerebral aneurysm using their own wall mechanical properties, 2013 (2013).

[35] A. Valencia, D. Ledermann, R. Rivera, E. Bravo, M.J.I.J.f.n.m.i.f. Galvez, Blood flow dynamics and fluid–structure interaction in patient-specific bifurcating cerebral aneurysms, 58(10) (2008) 1081-1100.

[36] Y. Wang, X. Leng, X. Zhou, W. Li, A.H. Siddiqui, J.J.W.n. Xiang, Hemodynamics in a middle cerebral artery aneurysm before its growth and fatal rupture: Case study and review of the literature, 119 (2018) e395-e402.

[37] G.K. Wong, W.J.J.o.C.N. Poon, Current status of computational fluid dynamics for cerebral aneurysms: the clinician's perspective, 18(10) (2011) 1285-1288.

[38] J. Xiang, S.K. Natarajan, M. Tremmel, D. Ma, J. Mocco, L.N. Hopkins, A.H. Siddiqui, E.I. Levy, H.J.S. Meng, Hemodynamic–morphologic discriminants for intracranial aneurysm rupture, 42(1) (2011) 144-152.

[39] A. Ziegler, U.J.B.J.J.o.M.M.i.B. Grömping, The generalised estimating equations: A comparison of procedures available in commercial statistical software packages, 40(3) (1998) 245-260.

[40] K.M.J.P.o.t.I.o.M.E. Saqr, Part H: Journal of Engineering in Medicine, Computational fluid dynamics simulations of cerebral aneurysm using Newtonian, power-law and quasi-mechanistic blood viscosity models, 234(7) (2020) 711-719.

[41] M. Saeedi, A. Shamloo, A.J.J.o.v.r. Mohammadi, Fluid-Structure Interaction Simulation of Blood Flow and Cerebral Aneurysm: Effect of Partly Blocked Vessel, 56(6) (2019) 296-307.